Korean J. Chem. Eng., 38(11), 2195-2207 (2021)
DOI: 10.1007/s11814-021-0936-8

pISSN: 0256-1115
eISSN: 1975-7220

Thermo-economic evaluation of R1233zd(E) as an R245fa alternative in organic Rankine cycle for geothermal applications

Gang Li[*,**,***,†]

*Ingersoll Rand Residential Solutions, 6200 Troup Highway, Tyler, TX 75707, United States
**Ingersoll Rand Engineering and Technology Center-Asia Pacific, Shanghai 200051, PR China
***School of Energy and Power Engineering, University of Shanghai for Science and Technology, Shanghai 200093, China
(*Received 11 March 2021 • Revised 4 August 2021 • Accepted 24 August 2021*)

Abstract−To quicken the process for high global warming potential (GWP) working fluid replacement for organic Rankine cycle (ORC) systems, a thermo-economic evaluation of low GWP fluid R1233zd(E) as an R245fa alternative has been performed in comparison with other natural fluids n-Pentane, Isopentane, and Isobutane for geothermal applications. The heat source water mass flow rate remains constant and 5 K pinch point is set for both evaporator side and condenser side. All working fluids have a close net thermal efficiency within 2%. Increasing the heat source from 120 °C to 160 °C gives a more than 20% efficiency rise. The low critical temperature of Isobutane limits its application for 160 °C heat source. R1233zd(E) displays a close mass flow rate (within 2%) from R245fa and others exhibit more than 40% flow rate reduction. The component level performance has also been investigated in this study. All alternatives exhibit a lower evaporator side (evaporator and preheater) heat transfer area than baseline R245fa, and a slightly higher condenser side (condenser and desuperheater) heat transfer area. For turbine performance, R245fa displays the highest volume flow ratio, indicating a significant change of the rotor blade height should be made between the inlet and outlet point for the expansion process. R1233zd(E) displays ~10% increase for turbine size parameter from baseline, n-Pentane shows ~22% rise, Isopentane exhibits ~11% rise, while Isobutane presents 32% decrease, respectively. In general, R1233zd(E) only exhibits ~2.3% higher specific investment cost than R245fa, while n-Pentane and Isopentane exhibit more than 15% cost rise. Thus, from the thermo-economic scale with an extended application range, R1233zd(E) exhibits a better overall performance index when compared with other R245fa alternatives and can be serviced as promising candidate to replace R245fa.

Keywords: R1233zd(E), Low Global Warming Potential, Geothermal, Thermo-economic

INTRODUCTION

Increasing fossil fuel consumption and greenhouse gas (GHG) emissions have brought various challenges such as ozone layer depletion, ecosystem destruction, air pollution and threatening human health. The rising energy cost, volatility in energy prices, and security of energy supply add to the complexity of such challenges. There is an alarming concern for the engineering community to explore approaches to resolve or relieve at the largest such energy and environmental issues. In fact, various countries, such as the European Union (EU), are aiming to cut the emissions. EU has set a goal with cutting the emissions significantly by 80-95% from 1990 levels as part of the efforts for a commitment to global climate action required by developed countries by 2050 [1]. In general, there are several approaches to achieve such targets, such as developing and utilizing renewable energy for power generation, and enhancing energy conservation system. Renewable and sustainable resources, including solar, biomass, and geothermal, can play a vital role in shifting the consumption of the high emission primary energy source such as fossil fuels [2].

Various cycles have been developed to utilize the renewables and waste heat, such as steam Rankine cycle, Brayton cycle, Stirling cycle and organic Rankine cycle (ORC). Compared with the conventional Rankine cycle, ORC can use volatile organic liquids to replace water. The low boiling point of volatile organic liquids can make ORC to be possible to recover the available heat from low temperature waste heat resources. What's more, its high flexibility, low maintenance cost, and good thermal properties have made ORC competitive to other cycles. Among various working fluids, the most widespread ones for ORC applications, such as geothermal plants or low temperature waste heat utilization, are R245fa, R123, and R134a. Muhammad et al. [3] investigated R245fa as a working fluid in a standard ORC system with the 120 °C steam waste heat as the heat source, and a commercial 1 kW scroll expander was applied. The heat exchangers are the plate heat exchanger type. The results showed that the maximum of the net thermal cycle efficiency can be obtained with a value of 4.66%. Li et al. [4] studied R123 as a working fluid in a recuperative cycle configuration. A rated power of 6 kW was employed and the heat source functioned by an electric resistance heater via a thermal oil loop with the flowing temperature of 130 °C. The results showed that a net cycle efficiency of 7.98% can be achieved. Generally, the average ORC thermal efficiency is in the range of 0.02 to 0.19.

Nevertheless, the environmental issues raise an increasing alarm

†To whom correspondence should be addressed.
E-mail: gangli166@gmail.com

to quicken the process for high global warming potential (GWP) working fluid replacement [5,6]. R123, which belongs to the family of hydrochlorofluorocarbons (HCFCs), is the second-generation working fluid with non-zero ozone depletion potential. R134a and R245fa, are in the family of hydrofluorocarbons (HFCs). R134a has a high GWP value of 1,300 and R245fa has a high value of 1,030. HFCs are the third-generation refrigerants and they have no effect on the ozone layer. Though the current refrigerant market is dominated by HFCs, the global regulations are now aiming at phasing down such high GWP HFCs [7]. For the current study, geothermal application was mainly investigated, and R245fa is the dominant working fluid in the market. In recent years, a series of new next-generation working fluids, such as hydrofluoroolefins (HFOs, i.e., fluorinated propene (propylene) isomers), have been developed. Such fluids have a low GWP and similar thermodynamic properties compared to the traditional working fluids.

Various studies concerning HFOs from both the simulation approaches and experimental aspects have been conducted to replace R245fa. Liu et al. [8] calculated the thermodynamic properties using the Peng-Robinson equation of state and the molecular based Joback method and investigated the HFOs with application in a standard ORC. This study concluded that HFO (R1234yf and R1225ye(E)) could achieve a better performance of thermal efficiency than the baseline fluids R245fa and R134a with a heat source of 120 °C to 150 °C low-grade heat. As for R1234yf, it is preferable for ~120 °C geothermal heat source temperature and the cycle efficiency can be freed from the pinch point limitation. Moles et al. [9] performed a numerical ORC investigation for R245fa, R1233zd(E) and R1336mzz(Z) under various operating conditions. A constant heat rate to the high pressure side evaporator was employed. Both the standard and the recuperated cycle were investigated. Their report indicated that R1233zd(E) has a 10.6% higher net cycle efficiency than the baseline R245fa. R1336mzz(Z) could obtain up to 17% higher net cycle efficiency than R245fa over the operating condition range. In addition, R1336mzz(Z) cycle efficiency is benefitted substantially by a recuperator. A recuperative supercritical ORC [10] was investigated with nontoxic fluids under various turbine inlet operating conditions. This study concluded that R1233zd(E) has the best plant efficiency of 16.2% and a second law efficiency of 52.3% under the turbine inlet condition of 240 °C. Chen et al. [11] proposed a novel ORC with a vapor-liquid ejector (EORC) to enhance the system performance. Results showed that the novel system can achieve a higher system efficiency than a conventional ORC and a regenerative organic Rankine cycle (RORC). They concluded that R1233zd(E) can be a good working fluid since it has a better system efficiency than R1336mzz(Z) and is more favored from the environmental aspects than R123. Longo et al. [12] conducted a thermodynamic performance evaluation of low-GWP refrigerants for heat pump (HP) and ORC applications. R1234ze(Z) displays a similar efficiency to R245fa, while R1233zd(E) exhibits a higher value and R600a a lower one than R245fa in both HP and ORC applications, respectively. Giuffrida [13] conducted a theoretical investigation of R1234ze(Z) and R1233zd(E) to replace R245fa in a micro ORC system. R1234ze(Z) and R1233zd(E) exhibit equal and better performance than R245fa, respectively, in their study. In addition, there is one review work [14] for different ORC fluids toward cycle configuration and operating condition. As for the experimental aspects, several studies have been published. The experimental work by Datla and Brasz [15] was performed for R1233zd(E) in a 75 kW standard ORC to replace R245fa. A radial inflow turbine was employed. At one operating point, R1233zd(E) could achieve an 8.7% net cycle efficiency. Another experimental study by Eyerer et al. [16] analyzed the applicability of R1233zd(E) to replace R245fa in existing systems. A scroll compressor was employed as an expander. Results show that R1233zd(E) performs 6.9% better than R245fa for the maximum value of thermal efficiency. The test was investigated by Molés [17] via a fully monitored ORC test rig, and the mass flow rate for R1233zd(E) was approximately 20% lower than for R245fa. This study concluded that the net electrical efficiency between the two working fluids is similar, ranging from 5% to 9.7%. They also revealed that R1233zd(E) has a higher value of maximum expander isentropic performance than R245fa, and they had a similar overall efficiency of the expander, ranging from 44% to 57% during the test. More recently, an experimental test by Yang et al. [18] was conducted under extensive operating conditions. During their test, R1233zd(E) led to approximately 3.8% higher than R245fa for the performance of the maximum cycle thermal efficiency. The former fluid could also achieve 4.5% higher maximum output electrical power than the latter. They concluded that R1233zd(E) can be an appropriate alternative to R245fa. Their following study [19] for the performance comparison between HFOs (R1234ze(Z), R1233zd(E), and R1336mzz(E)) and baseline R245fa also recommended that R1233zd(E) proved to be an appropriate alternative to R245fa. Further study by Eyerer et al. [20] also revealed that R1233zd(E) can lead to a close thermal efficiency to R245fa. Talluri et al. [21] conducted an experimental study of a Tesla turbine with a refrigerant of R1233zd(E). Results showed that a maximum net power delivery could be obtained with a value of 371W, demonstrating the feasibility of utilizing Tesla turbines in ORC applications. A maximum shaft efficiency could be obtained as 9.62% and a maximum adiabatic efficiency could reach 30%. They also investigated the geometry for Tesla turbine performance for ORC applications [22].

Based on the literature review work, all the aforementioned simulation approaches and experimental studies conducted much of the applicability work of R1233zd(E) as a drop-in replacement to R245fa in ORC system. Nevertheless, there is a lack of the heat transfer area evaluation and economic prediction aspects. Most previous studies and associated conclusions were derived strictly based on thermodynamic cycle analyses and they do not give enough consideration for the component performance between the heat source/sink and corresponding fluids (R1233zd(E) and R245fa) in the ORC heat exchangers. In addition, the system cost should be considered together with the thermal performance aspects to have an overall evaluation for R1233zd(E) as a new refrigerant to replace R245fa. What's more, in the past studies, R1233zd(E) was not compared for thermo-economic performance in detail in ORCs with non-synthesized fluids, such as benzene and toluene. Thus, and, by extension, the current study performed a thermo-economic evaluation for R1233zd(E) and several non-synthesized fluids as R245fa alternatives from both the system level thermal performance and system components' (heat exchangers, turbines) sizes and costs as

well, leading to a well-defined analysis of the benefits and points of employing new working fluids in ORC systems. It is anticipated that the viewpoints from this study can be beneficial for engineers, policy-makers, and manufacturers to maintain the maximum system thermal performance delivery with consideration of economic benefits as well.

This paper is organized as follows: Section 2 introduces the working fluid selection and comparison. Section 3 shows the ORC system description, and Section 4 introduces the ORC thermodynamic model, heat transfer and component size model, component cost model and performance evaluation methodology. Section 5 discusses the results for thermo-economic performance. Section 6 summarizes the perspectives, directions and conclusions towards the sustainable target.

PROPERTIES OF REFRIGERANTS SELECTED

Table 1 is a comparison of the main characteristics between baseline R245fa, R1233zd(E) and several natural refrigerants [23]. All R245fa alternatives can provide a more than 99% GWP reduction from baseline R245fa. R1233zd(E) is normally described as zero-ozone depletion potential (ODP) due to its very low and negligible ODP, less than 0.0004.

The normal boiling point (NBP) of R1233zd(E) is close to that of R245fa. n-Pentane and Isopentane exhibit a higher critical temperature from the baseline, while Isobutane presents a lower one. In addition, several natural fluids have the high risk of flammability (A3 level). Fig. 1 shows the comparison in saturation temperature-entropy diagrams (i.e., T-s diagram) and the vapor pressure comparison of refrigerants in log P-($-T_{sat}^{-1}$) diagrams for different fluids. From such figures, it can be found that R1233zd(E)'s vapor pressure is close to R245fa and is above atmospheric pressure when the condensing temperature is 30 °C. While, when condensing temperature decreases, other natural fluids such as n-Pentane and Isopentane will be at the risk of having pressure lower than atmospheric pressure. The vapor saturation curves of R245fa and R1233zd(E) show a slight positive slope and can be classified as dry-isentropic fluids and others are regarded as dry fluids.

ORC SYSTEM DESCRIPTION

Fig. 2 shows the basic ORC cycle with four basic processes: heat addition, expansion, heat rejection and pumping. For the basic cycle, it is sub-critical and non-regenerative. For the heat addition process, there are two heat exchangers: the preheater, which is used to pre-heat the working fluid to the saturated state liquid, and the evaporator, which is used to evaporate the fluid to the saturated vapor or superheated state if necessary. There are also two other heat exchangers for the heat rejection process: the desuperheater, which is used to cool the working fluid from the superheated vapor state to the saturated vapor, and the condenser, which is used to condensate the fluid to the saturated liquid. All heat exchangers are counter-current shell and tube heat exchangers.

MODELS AND METHODOLOGY

In this section, different models for ORC thermodynamic process, heat transfer process, component sizing and cost, are presented.

Table 1. Main characteristics of R245fa, R1233zd(E), n-pentane, isopentane, and isobutane

	R245fa	R1233zd(E)	n-Pentane	Isopentane	Isobutane
Molecular mass (g/mol)	130.5	134	72.15	72.15	58.123
ASHARE Std 34 safety class	B1	A1	A3	A3	A3
ODP	0	<0.0004	0	0	0
AR5 $GWP_{100\text{-year}}$	1030	1	5	5	3
Critical temperature (°C)	154.01	165.6	196.55	187.2	134.66
Critical pressure (MPa)	3.651	3.623	3.3675	3.378	3.629
NBP (°C)	14.81	17.97	36.21	27.78	−12
Flammability	Non-flammable	Non-flammable	Flammable	Flammable	Flammable
Slope	Dry-isentropic	Dry-isentropic	Dry	Dry	Dry
Evaporating pressure at 120 °C (MPa)	1.930	1.575	0.90	1.086	2.836
Condensing pressure at 30 °C (MPa)	0.178	0.155	0.082	0.1091	0.4047
Liquid density[a] (kg/m^3)	1,324.788	1,250.597	616.1405	609.844	544.310
Vapor density[a] (kg/m^3)	10.102	8.508	2.439	3.277	10.480
Liquid c_P[a] (kJ/kg·K)	1.329	1.224	2.339	2.300	2.463
Vapor c_P[a] (kJ/kg·K)	0.919	0.839	1.724	1.726	1.835
Liquid therm. cond.[a] (mW/m·K)	86.540	81.252	110.091	100.187	87.489
Vapor therm. cond.[a] (mW/m·K)	13.0515	11.0759	14.9817	14.8566	17.3706
Liquid viscosity[a] (μPa s)	374.770	272.288	210.493	208.875	143.432
Vapor viscosity[a] (μPa s)	10.580	10.497	6.839	7.130	7.630
Latent heat[a] (kJ/kg)	187.4	189.1	362.4	340.9	323.4
Latent heat at NBP (kJ/kg)	196.901	194.767	357.583	343.321	365.322

[a]Under 30 °C conditions. All properties were obtained using REFPROP [23]

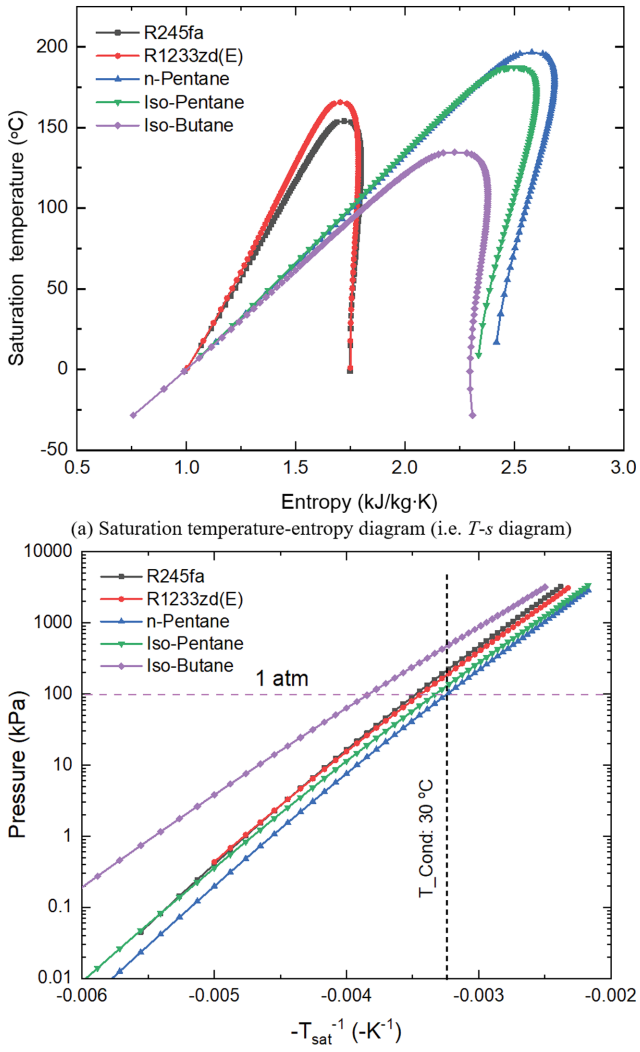

(a) Saturation temperature-entropy diagram (i.e. *T*-*s* diagram)

(b) Vapor pressure of refrigerants in log *P*-(-T_{sat}^{-1}) diagram

Fig. 1. Refrigerant property diagram comparison.

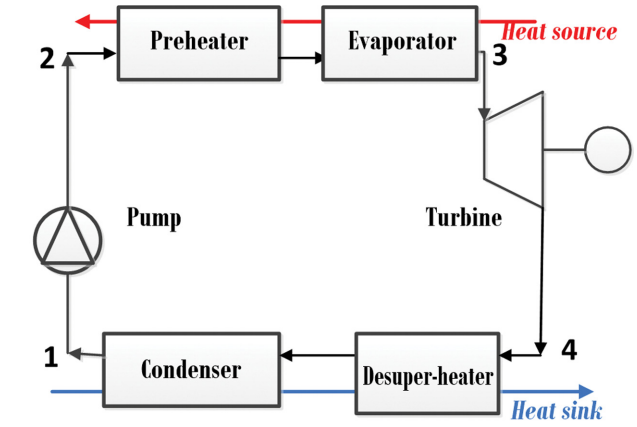

(a) Organic Rankine baseline cycle

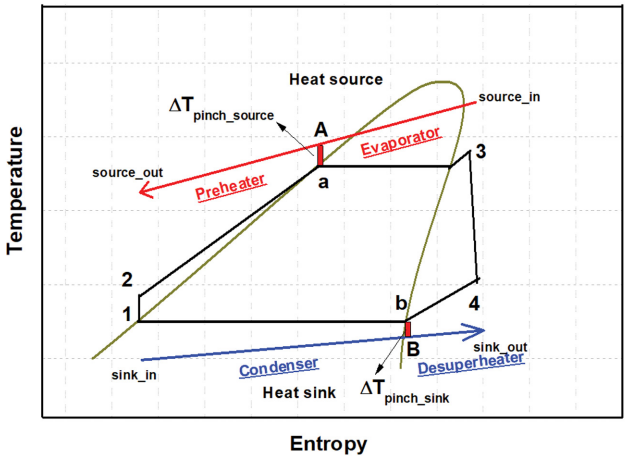

(b) T-s diagram for organic Rankine baseline cycle

Fig. 2. Schematics of organic Rankine baseline cycle.

In addition, the performance evaluation methodology is also revealed.

1. ORC Thermodynamic Model

As shown in Fig. 2, the pump power W_p, which is pumping the fluid from saturated liquid point 1 to high pressure state point 2, is calculated as:

$$W_p = \dot{m}(h_2 - h_1) = \dot{m}(h_{2s} - h_1)/\eta_p \quad (1)$$

η_p is the isentropic efficiency for the pump and $\dot{m}$ is the organic fluid mass flow rate.

The heat source $\dot{Q}_{source}$ is obtained as:

$$\dot{Q}_{source} = \dot{m}(h_3 - h_2) = \dot{m}_{source}(h_{source,\,in} - h_{source,\,out}) \quad (2)$$

$$\dot{Q}_{source} = \dot{Q}_{evaporator} + \dot{Q}_{preheater} \quad (3)$$

$\dot{m}_{source}$ is the source fluid mass flow rate and the heat addition can be divided into two parts: evaporator side $\dot{Q}_{evaporator}$ and the preheater side $\dot{Q}_{preheater}$. The calculation for each side is shown as follows:

$$\dot{Q}_{evaporator} = \dot{m}(h_3 - h_a) = \dot{m}_{source}(h_{source,\,in} - h_A) \quad (4)$$

$$\dot{Q}_{preheater} = \dot{m}(h_a - h_2) = \dot{m}_{source}(h_A - h_{source,\,out}) \quad (5)$$

$$\Delta T_{pinch,\,source} = T_A - T_a \quad (6)$$

$\Delta T_{pinch,\,source}$ is the pinch temperature difference at the heat source side.

The cycle power W_t generated as the working fluid is expanded from state point 3 to state point 4 is given by:

$$W_t = \dot{m}(h_3 - h_4) = \dot{m}(h_3 - h_{4s}) \cdot \eta_t \quad (7)$$

η_t is the isentropic efficiency for the turbine.

After expansion, the heat rejection process begins. Similarly, the heat rejection $\dot{Q}_{sink}$ from the heat source is given by:

$$\dot{Q}_{sink} = \dot{m}(h_4 - h_1) = \dot{m}_{sink}(h_{sink,\,out} - h_{sink,\,in}) \quad (8)$$

$$\dot{Q}_{sink} = \dot{Q}_{desuperheater} + \dot{Q}_{condenser} \quad (9)$$

$\dot{m}_{sink}$ is the heat sink fluid mass flow rate and the heat rejection can be divided into two parts: desuperheater side $\dot{Q}_{desuperheater}$ and the condenser side $\dot{Q}_{condenser}$. The calculation for each side is shown as follows:

$$\dot{Q}_{desuperheater} = \dot{m}(h_4 - h_b) = \dot{m}_{sink}(h_{sink,\,out} - h_B) \quad (10)$$

$$\dot{Q}_{condenser} = \dot{m}(h_b - h_1) = \dot{m}_{sink}(h_B - h_{sink,\,in}) \quad (11)$$

$$\Delta T_{pinch,\,sink} = T_b - T_B \tag{12}$$

The total net work delivery W_{net} is given by:

$$W_{net} = W_t - W_p \tag{13}$$

System thermal efficiency η is calculated as:

$$\eta = (W_t - W_p)/\dot{Q}_{source} \tag{14}$$

All the thermodynamic models are listed in this section. For the heat addition process and heat rejection process, it is estimated 30-50 kPa pressure drop.

2. Heat Transfer and Component Sizing Model

For the current study, the heat exchangers are the shell and tube type with the counter-current flow configuration. There is one-pass in shell and two-pass in tubes. The heat source/heat sink fluid (i.e., water) is in the tube side and the organic or natural working fluid is in the shell side. An allowable pressure drop (<35 kPa in the current study) is recommended for heat exchangers during the heat transfer process.

Several basic assumptions are made as follows: fluid is steady and its properties are independent of time; the pressure at one point for the fluid is independent of direction; body force is only caused due to the gravity, and the heat losses to ambient are neglected.

2-1. Heat Exchangers

2-1-1. Tube Side Heat Transfer and Pressure Drop

For the tube side, it is the single phase state with water as the liquid. The tube cross flow area a_t and the mass flow per area unit $\dot{G}_t$ are listed by:

$$a_t = \frac{N_T \pi d_{in}^2}{4 N_{tp}} \tag{15}$$

$$\dot{G}_t = \frac{\dot{m}_t}{a_t} \tag{16}$$

N_T is the number of tubes for each heat exchanger, π is the math constant, d_{in} is the tube internal diameter, N_{tp} is the number of passes in tubes and $\dot{m}_t$ is the mass flow rate in the tube side, either from heat source fluid or heat sink fluid.

The Reynolds number Re_t in the tube side is calculated as,

$$Re_t = \frac{\dot{G}_t d_{in}}{\mu_t} \tag{17}$$

μ_t is the dynamic viscosity of the fluid in the tube.

The Prandtl number Pr_t and Nusselt number Nu_t read as follows:

$$Pr_t = \frac{C_{p,t}\mu_t}{\lambda_t} \tag{18}$$

$$Nu_t = 0.023 (Re_t)^{0.8} Pr_t^{n_{DB}} \tag{19}$$

$C_{p,t}$ is the fluid heat capacity. n_{DB} is the parameter of the Dittus-Boelter correlation. The correlation has a value of 0.3 when the fluid is cooling while 0.4 when it is heating [24]. The wall heat transfer coefficient h_t at the tube side can be obtained via

$$h_t = \frac{Nu_t \lambda_t}{d_{in}} \tag{20}$$

The heat transfer area $A_{HX\text{-}preset}$ is obtained by,

$$A_{HX\text{-}preset} = N_T L_{tube} (\pi d_{out}) N_s \tag{21}$$

L_{tube} is the tube length, d_{out} is the tube external diameter, and N_s is the number of shells per heat exchanger. In this work, the value is 1.

The pressure drop [25] in the tube side ΔP_t is calculated as,

$$\Delta P_t = \frac{\rho_t v_t^2}{2}\left(4 f_t \frac{L_{tube} N_{tp} N_s}{d_{in}} + 4 N_{tp} N_s\right) \tag{22}$$

f_f is the friction factor and v_t is the tube inside fluid velocity.

The friction factor f_t reads as follows:

$$f_t = \exp(0.576 - 0.19 \ln Re_t) \tag{23}$$

2-1-2. Shell Side Heat Transfer and Pressure Drop

This section discusses the shell side heat transfer and pressure drop. With the tube geometry determined, the total number of tubes N_T can be predicted in fair approximation as function of D_s by taking the shell circle and dividing it by the projected area of the tube layout pertaining to a single tube A_1,

$$N_T = (CTP)\pi D_s^2/(4A_1) \tag{24}$$

CTP is the tube count calculation constant [25]. The CTP value is 0.93 for one-tube pass, 0.90 for two-tube pass and 0.85 for three-tube pass, respectively. Here we choose two-tube pass.

$$A_1 = (CL) P_T^2 \tag{25}$$

P_T is the tube pitch and CL is the tube layout constant, with the value to be 1 for 90° and 45°, and 0.87 for 30° and 60°, respectively.

The cross-flow area a_s and mass flow per area unit $\dot{G}_s$ in that order are shown as,

$$a_s = \frac{D_s C_s B_s}{P_T N_{sp}} \tag{26}$$

$$\dot{G}_s = \frac{\dot{m}_s}{a_s} \tag{27}$$

C_s is the clearance between tubes, B_s is the baffle spacing, N_{sp} is the number of passes in shells and $\dot{m}_s$ is the mass flow rate in shell side.

The shell diameter D_s is calculated as,

$$D_s = D_b + C_s \tag{28}$$

D_b is the bundle tube diameter, given by,

$$D_b = d_{out}\left(\frac{N_T}{K_1}\right)^{(1/n_1)} \tag{29}$$

$$C_s = P_T - d_{out} \tag{30}$$

n_1 and K_1 are the coefficients depending on the tube pattern and number of tube passes [26]. The baffle position with perpendicular to the flow can help to produce high turbulence for the shell side [25], and the baffle spacing B_s is obtained via,

$$B_s = D_s/2 \tag{31}$$

The Reynolds number in the shell side Re_s is calculated as,

$$Re_s = \frac{\dot{G}_s D_{eq,s}}{\mu_s} \tag{32}$$

The equivalent diameter of shell, $D_{eq,s}$, is the function of tube pat-

tern, and for the square pitch type, it is,

$$D_{eq,s}=\frac{4P_t^2-\pi d_{out}^2}{\pi d_{out}} \tag{33}$$

For triangular pattern, it reads as follows:

$$D_{eq,s}=\frac{2P_t^2\sqrt{3}-\pi d_{out}^2}{\pi d_{out}} \tag{34}$$

The dimensionless Prandtl number Pr_s is given by,

$$Pr_s=\frac{C_{p,s}\mu_s}{\lambda_s} \tag{35}$$

For the shell side, the heat transfer calculation can be divided into three sub-sections:

(1) Single phase process for preheater and desuperheater.

It is assumed the baffle cut ratio is set to be 25% in this study. Based on study by Mc Adams [27], the shell side heat transfer coefficient h_s can be calculated as follows:

$$h_s=0.36\frac{k_s}{D_{eq,s}}Re_s^{0.55}\left(\frac{c_{p,s}\mu_s}{k_s}\right)^{1/3}\left(\frac{\mu_b}{\mu_w}\right)^{0.14} \tag{36}$$

μ_b is the viscosity evaluated at the bulk mean temperature, μ_w is viscosity evaluated at the wall temperature, $c_{p,s}$ is the shell side fluid specific heat at constant pressure, and k_s is the shell side fluid thermal conductivity.

The pressure drop for the shell side ΔP_s can be calculated as follows:

$$\Delta P_s=f_t\frac{\dot{G}_s^2(N_B+1)D_sN_sN_{sp}}{2\rho_s D_{eq,s}\varnothing_s} \tag{37}$$

N_B is the number of baffles, (N_B+1) is the number of times fluid passes to the tube bundle, $\varnothing_s=(\mu_b/\mu_w)^{0.14}$, and the shell side friction factor f_s is calculated as,

$$f_s=\exp(0.576-0.19\ln Re_t) \tag{38}$$

For which the friction factor should be considered for the range of the Reynolds number described as follows:

$$400<Re_s\leq 1\times 10^6 \tag{39}$$

(2) Evaporator side two phase boiling process

Different from the single phase heat transfer process, the two phase boiling process in the evaporator notices the significant changes of fluid properties. Based on the approximate modifications to the Dittus-Boelter type correlation, Tinker [28] proposed the coefficient in the saturated boiling region, and it is the sum of convective and nucleate components, given by,

$$h_s=h_{nuc}+h_{conv} \tag{40}$$

$$h_{conv}=0.023Re_L^{0.8}Pr_L^{0.4}(k_L/D_{eq,s})F_c \tag{41}$$

$$h_{nuc}=0.00122\left(\frac{k_L^{0.79}c_{p,L}^{0.45}\rho_L^{0.49}g_o^{0.25}}{\sigma^{0.5}\mu_L^{0.29}(\lambda\cdot\rho_v)^{0.24}}\right)(T_w-T_s)^{0.24}(P_w-P_s)^{0.75}S_c \tag{42}$$

Re_L and Pr_L are calculated on the assumption of liquid flowing in the shell with the consideration of the equivalent diameter of the shell. The subscripts L and v account for the liquid and gas phase. F_c is the convective-correction factor, which is the strictly the flow parameter. This factor is the ratio of the two-phase Reynolds number to the liquid Reynolds number based on the liquid fraction of the flow. (T_w-T_s) is the temperature superheat between the value under the wall condition and that under the fluid saturation condition, and (P_w-P_s) is the difference in vapor pressure corresponding to this superheat. σ is the vapor-liquid surface tension, λ is the latent heat of vaporization, g_o is the gravitational constant, and S_c is the suppression factor. S_c approaches unity at zero flow rate and zero at infinite flow rate, and it can be represented as a function of the local two phase Reynolds number.

For the pressure drop, here the pressure drop due to the friction and acceleration are mainly discussed. The pressure drop due to the friction [29] is,

$$\Delta P_{fr}=(1+(Y^2-1)[Bx^{(2-n)/2}(1-x)^{(2-n)/2}+x^{(2-n)}])\Delta P_{single} \tag{43}$$

where ΔP_{single} is the frictional, ideal pressure drop in the shell if all the fluid is saturated liquid, Y^2 is the Chisholm parameter, x is the quality of the fluid. For the cross flow B=1 and n=0.37, while for the window flow $B=(\rho_h/\rho_L)^{1/4}$ and n=0. ρ_h is the homogeneous flow density, given as,

$$\rho_h=\frac{1}{\frac{1-x}{\rho_L}+\frac{x}{\rho_v}} \tag{44}$$

The pressure drop due to the friction and acceleration is,

$$\Delta P_{ac}=\dot{G}_s^2\left\{\left(\frac{(1-x)^2}{\rho_L(1-\alpha)}+\frac{x^2}{\rho_v\alpha}\right)-\left(\frac{(1-x)^2}{\rho_L(1-\alpha)}+\frac{x^2}{\rho_v\alpha}\right)_{in}\right\} \tag{45}$$

where $\alpha=1/\left(1+\frac{1-x}{x}\frac{\rho_v}{\rho_L}\right)$ is the void fraction as calculated for a homogeneous flow.

(3) Condenser side two phase condensation process

Regarding the condensation process, the heat transfer coefficient is utilized from the study by Boyko and Kruzhilin [30]. The condensate in the condenser is assumed to form annular Flow.

First, the liquid flow based Reynolds number and Prandtl number are used for calculation as follows:

$$h_L=0.023Re_L^{0.8}Pr_L^{0.4}(k_L/D_{eq,s}) \tag{46}$$

Then the shell side convection heat transfer coefficient h_s can be calculated as,

$$h_s=\frac{h_L}{2}(1+\sqrt{\rho_L/\rho_v}) \tag{47}$$

The two-phase condensing process pressure drop is calculated by the same correlations as given for the evaporator.

Finally, for each sector, the overall heat transfer coefficient for clean surface $U_{c,sector}$ based on tuber external service is,

$$\frac{1}{U_{c,sector}}=\frac{1}{h_s}+\frac{1}{h_t}\cdot\frac{d_{out}}{d_{in}}+\frac{\ln(r_{out}/r_{in})r_{out}}{k_{tube}} \tag{48}$$

k_{tube} is the thermal conductivity of the tube material. When the fouling resistance is considered (R_{fi}), the heat transfer coefficient for fouled surface $U_{f,sector}$ can be calculated via:

$$\frac{1}{U_{f,\,sector}}=\frac{1}{U_{c,\,sector}}+R_{ft} \tag{49}$$

The fouling resistance can be checked from the Table in Reference [31]. Here the refrigerant side fouling resistance is pre-set as 0. Therefore, with $U_{f,sector}$ obtained, the heat exchanger heat transfer area for each sector $A_{HX,sector}$ can be obtained via,

$$A_{HX,sector}=Q_{HX,sector}/(U_{f,sector}\cdot LMTD_{sector}\cdot F_{T,sector}) \tag{50}$$

$A_{HX,sector}$ is the heat transfer area for the corresponding sector, $Q_{HX,sector}$ is the heat flow for that sector, $F_{T,sector}$ is the sector temperature factor correction, and $LMTD_{sector}$ is the sector log-mean temperature difference, which can be easily obtained from inlet and outlet temperature for hot and cold fluids.

Choose proper setting for sector geometry such as shell diameter and tube length for each sector sub heat exchanger, and make sure δ is in the range of 0 to 10%. For a fair comparison, all working fluids should have a close value of δ.

$$\delta=(A_{HX,sector}-A_{HX,sector\text{-}preset})/A_{HX,sector} \tag{51}$$

$A_{HX,sector\text{-}preset}$ is the heat exchanger area from Eq. (21), $A_{HX,sector}$ is the sector heat exchanger area from Eq. (50), and δ is the relative ratio of heat exchanger area. With a satisfied value for δ within the needed range, the sector heat transfer performance and heat transfer area can be obtained. In this way, the sector can be obtained for heat exchanger performance. Finally, the overall heat exchanger area $A_{HX,overall}$ is,

$$A_{HX,overall}=A_{HX,single}+A_{HX,twophase} \tag{52}$$

For current study, the horizontal orientation is chosen and the tube is the plain type with a layout angle 30° and a wall thickness is 2.2 mm. The tube material is the 304 stainless steel (18Cr, 8Ni). The thermal fluid process condition inputs are determined from section *ORC thermodynamic model* for water side/refrigerant side pressure/temperature/vapor quality/mass flow rate conditions. The heat exchanger thermal calculation is based on pre-set condition. The fluid information can be obtained from the fluid package REFPROP.

2-2. Turbines

For the current cycle configuration, there is only one turbine. It is the main component for power generation delivery. In fact, the volume flow ratio (V_R, see below) has a major impact on turbine efficiency and component geometry. Usually a high value indicates the expansion process with the corresponding fluid necessitates a large change in rotor blade height between the inlet and outlet points.

$$V_R=\rho_{in}/\rho_{out} \tag{53}$$

The size parameter SP (see equation below) is the turbine size indicator based on the reference [31]. In fact it can also be used in a similar fashion to the specific diameter [32,33].

$$SP=\sqrt{V_{out,\,is}}/\sqrt[4]{\Delta h_{is}} \tag{54}$$

$V_{out,is}$ is the volume flow ratio of the outlet streams of the turbine. Δh_{is} is the isentropic specific enthalpy drop in the turbine.

In this section, it is necessary to explain why the component-specific performance should be considered. Under the same operating condition (same heat source/sink level and pinch point setting), when the old refrigerant such as R245fa is phased out and the low GWP fluids are adopted, the original components (such as heat exchangers and turbines) are usually not very qualified for the new low GWP fluids. The comparison for the component performance can quantitatively provide suggestions for the manufacturers to select the component size from their existing or new supplier database.

3. Component Cost Model and Performance Evaluation Methodology

This section mainly discusses economic modeling, mainly about the component cost. Key components, such as fluid pump, the turbine, and the heat exchangers, can give a general estimation of the capital cost. Though such cost does not involve the installation cost, it can still give the instructions for working fluid selection. The cost for other factors for the total installation cost can be similar and their effect on the installation cost is manifested directly. For the working fluid with a high flammability, the additional cost due to safety protection should be considered. In fact, there always exists inherent uncertainties for the estimation for the cost for different components. However, with a single and consistent reference source of information for the system cost, comparison for different working fluids is more reasonable.

Here the main method from reference [34] is considered, and an appropriate modification for this method is performed for the component cost evaluation. The bare module corresponding to each component is associated with the base cost. Regarding inflation, it is calculated from Chemical Engineering Plant Cost Index (CEPCI) [35].

The base costs for heat exchangers, pumps and turbines are calculated as follows,

$$\log C_{b.HX}=K_{1.HX}+K_{2.HX}\log(A_{HX})+K_{3.HX}[\log(A_{HX})]^2 \tag{55}$$

$$\log C_{b,pump}=K_{1,pump}+K_{2,pump}\log(W_p)+K_{3,pump}[\log(W_p)]^2 \tag{56}$$

$$\log C_{b.turbine}=[K_{1.turbine}+K_{2.turbine}\log(W_t)+K_{3.turbine}[\log(W_t)]^2]\varphi \tag{57}$$

$C_{b.HX}$, $C_{b,pump}$ and $C_{b.turbine}$ are the base cost for the heat exchangers, pumps and turbines, with the unit dollar, correspondingly. A_{HX} is the area of each heat exchanger, as discussed in section *Heat transfer and component sizing model* and W_p is the pump power. W_t is the turbine power generation. K_1, K_2, and K_3 with the sub (such as HX, pump, and turbine) are coefficient values related to the corresponding component. φ is the turbine size ratio to the baseline R245fa. This has not been discussed in detail in the open literature for turbine cost evaluation. The existing studies do not involve the value of φ. In fact, with the same turbine power delivery for different working fluids, the cost of turbine should be different due to the different turbine size (turbine size parameter-SP, which is discussed in section *Heat transfer and component sizing model*). In current study, φ is the ratio of new working fluid SP to the baseline R245fa SP. For R245fa, φ is 1.

Then the purchase cost of the component C_{sub} is calculated as,

$$C_{sub}=C_{b.c}\cdot[CEPCI_{2019}/CEPCI_{2001}]\cdot F_{BM} \tag{58}$$

$C_{b.c}$ is the base cost for the component, such as $C_{b.HX}$, $C_{b,pump}$ or $C_{b.turbine}$. Inflation is also considered and calculated from Reference [35]. $CEPCI_{2019}$ is the Chemical Engineering Plant Cost Index

Table 2. Coefficient for the component cost functions

Component	X	Component subscript c for cost calculation	Coefficient for component								
			$K_{1,c}$	$K_{2,c}$	$K_{3,c}$	$B_{1,c}$	$B_{2,c}$	$F_{M,c}$	$C_{1,c}$	$C_{2,c}$	$C_{3,c}$
Turbine	W_t (kW)	turbine	2.7051	1.4398	-0.1776	-	-	-	-	-	-
Shell-and-tube heat exchanger	A_{HX} (m^2)	HX	4.3247	-0.303	0.1634	1.63	1.66	1.81		F_P=1.25	
Pump-volumetric type	W_p (kW)	pump	3.4771	0.1350	0.1438	1.89	1.35	1.6	-0.245382	0.259016	–0.01363

* For the current study, the F_{BM} for turbine is set to be 3.5.

(CEPEI) for year 2019 with a value of 607.5 and $CEPCI_{2001}$ is for year 2001 with a value of 397, respectively. F_{BM} is the bare module factor, given by,

$$F_{BM}=B_1+B_2 \cdot F_P \cdot F_M \quad (59)$$

B_1 and B_2 are coefficients related to the component, as shown in Table 2. F_M is the material factor peculiar for each material different from the basic one, and F_P is the pressure factor, given by,

$$\log F_P=C_1+C_2\log(P)+C_3[\log(P)]^2 \quad (60)$$

P is the pressure with the unit bar for calculation. For some component, F_M is given, and the coefficient (C_1, C_2 and C_3) for the component cost functions is shown in Table 2.

The sum of the total component cost is given by C_{totab}

$$C_{total}=\omega \Sigma C_{sub} \quad (61)$$

Regarding the hydrocarbon fluids (n-Pentane, Isopentane, and Isobutane), an additional cost should be considered for flammability issues. ω is the flammability factor; for non-flammable refrigerants, it is 1 and for flammable refrigerants, it is pre-set as 1.1.

Then the specific investment cost (SIC) could be obtained as follows:

$$SIC=C_{total}/W_{net} \quad (62)$$

RESULTS AND DISCUSSION

In this section, different performance index, such as system level thermal performance, component level heat exchanger size and turbine size, and economic performance are discussed. In this study, the heat source water flow rate remains constant (23 kg/s) and 5 K pinch point is set for both evaporator side and condenser side. The isentropic efficiency for both of the pump and turbine is set to be 75%.

1. ORC Thermal Performance for Different Working Fluids

Fig. 3 demonstrates the variation of the ORC system level performance under different refrigerants. Under the same level of heat source, all working fluids have a close net thermal efficiency within 2%. For R245fa, a 10.5% net thermal efficiency increase can be achieved when the heat source is increased from 120 °C to 140 °C, and a ~22% increase can be obtained from 120 °C to 160 °C. Similarly, all other fluids can give a ~10% thermal efficiency increase under the 140 °C heat source, and ~20% rise under the 160 °C heat source (160 °C heat source performance data is not shown for Isobutane due to its lower critical temperature and cannot achieve 5 K

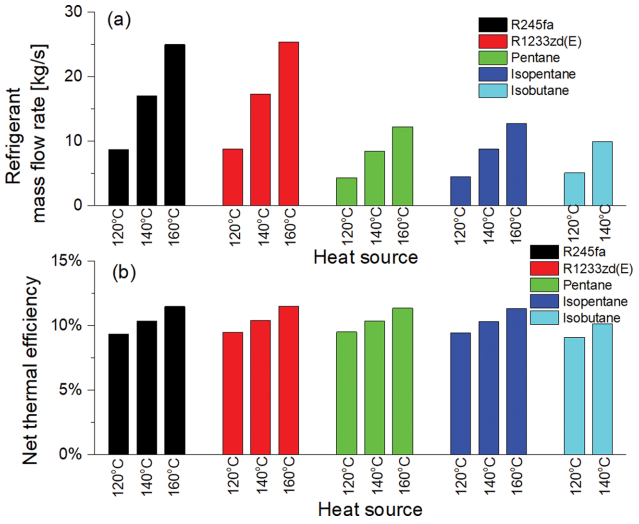

Fig. 3. System level performance under different refrigerants.

pinch point for the evaporator side), respectively. Regarding the mass flow rate under the same heat source level, all non-synthesized working fluids exhibit a lower value from baseline R245fa, ~50% decrease for n-Pentane and Isopentane, and ~40% reduction for Isobutane. R1233zd(E) displays a close mass flow rate value (within 2%) to R245fa. Also, heat source of 140 °C offers a double value of mass flow rate from that of 120 °C and heat source of 160 °C provides a triple one. In addition, the system level simulation results for different working fluids are presented in Table 3. It can be noted that under the same heat source level, Isobutane displays a highest value of pressure for evaporator or condenser while n-Pentane the lowest. n-Pentane and Isopentane exhibit a lower turbine inlet fluid density. Isobutane displays the lowest net-power generation delivery.

2. ORC Component Sizing Comparison for Different Working Fluids

In this section, the component sizing comparison for different working fluids are discussed. During the initial simulation, the refrigerant side shell internal diameter is pre-set as 1,750 mm (lower or higher with) for evaporator and condenser with a reasonable range of tube length. With proper adjustment and arrangement for geometry for shell and tube heat exchangers, all fluids can achieve a close value for δ. The heat transfer area performance is mainly discussed for evaporator side (evaporator and preheater) and condenser side (condenser and desuperheater) with R245fa and its alternatives. The tube side is water with sensible state and its heat

Table 3. System level simulation results under different refrigerants

Heat source:	Working fluid	Evaporating temperature [°C]	Evaporating pressure [MPa]	Condensing temperature [°C]	Condensing pressure [MPa]	Turbine inlet temperature [°C]	Turbine inlet density [kg/m^3]	Net power generation [kW]	Condenser water flow rate [kg/s]	Net thermal efficiency
120 °C	R245fa	102.58	1.34	43.89	0.28	107.58	14.77	182.38	42.21	0.094
	R1233zd(E)	101.81	1.08	44.04	0.24	106.81	12.44	184.86	42.15	0.095
	Pentane	101.52	0.61	43.56	0.13	106.52	3.45	185.14	42.15	0.095
	Isopentane	101.86	0.75	43.45	0.17	106.86	4.50	184.23	42.19	0.095
	Isobutane	103.74	2.13	43.81	0.59	108.74	13.98	176.89	42.34	0.091
140 °C	R245fa	112.61	1.66	43.75	0.28	117.61	14.68	404.71	83.86	0.104
	R1233zd(E)	110.51	1.30	43.94	0.24	115.51	12.34	407.51	83.79	0.104
	Pentane	109.60	0.73	43.44	0.13	114.6	3.40	405.81	83.83	0.104
	Isopentane	110.47	0.90	43.32	0.17	115.47	4.43	403.32	83.89	0.103
	Isobutane	116.51	2.67	43.68	0.58	121.51	13.88	396.30	84.06	0.101
160 °C	R245fa	126.86	2.21	43.62	0.28	131.86	14.47	677.98	124.81	0.115
	R1233zd(E)	122.06	1.64	43.81	0.24	127.06	12.22	677.61	124.82	0.115
	Pentane	119.73	0.90	43.22	0.13	124.73	3.34	669.69	125.01	0.114
	Isopentane	121.40	1.12	43.07	0.17	126.4	4.34	667.23	125.07	0.113
	Isobutane	-	-	-	-	-	-	-	-	

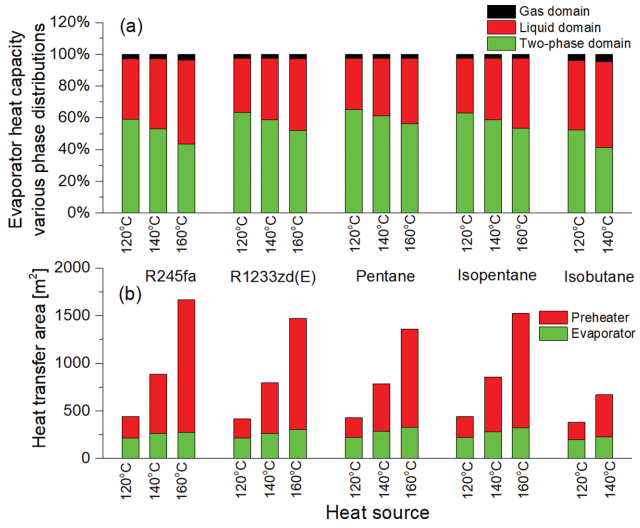

Fig. 4. Evaporator side heat transfer area performance under different refrigerants.

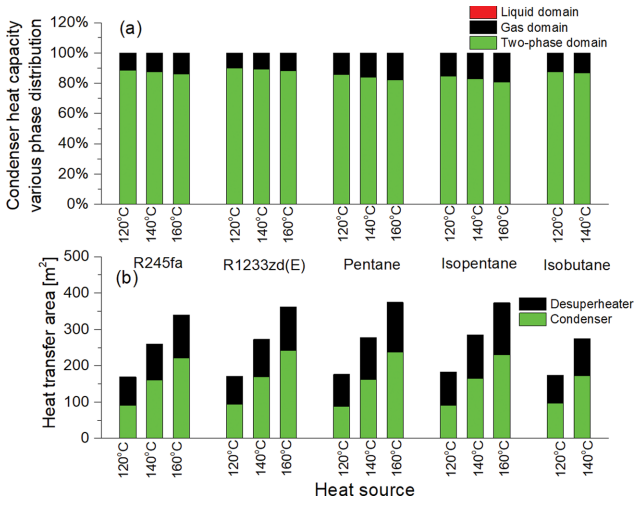

Fig. 5. Condenser side heat transfer area performance under different refrigerants.

transfer performance does not vary much for the heat exchanging processes.

2-1. Heat Exchangers

The heat transfer area performance for different heat exchangers is shown in Fig. 4 and Fig. 5. From Fig. 4 it can be found that the area of the evaporator for different working fluids is close (within 4%) except for Isobutane. Isobutane exhibits ~8% heat transfer area reduction from the baseline R245fa. This can be explained from the phase domains in Fig. 4. The two-phase domain for Isobutane is relatively lower than other fluids under the same heat source levels. It is 52% for two-phase domain for Isobutane while it is above 60% for other fluids under the 120 °C heat source, and a similar trend is exhibited for other heat source. The heat transfer area of the preheater is more pronounced than that of the evaporator, especially for a higher heat source. In general, all other fluids can provide a lower total heat transfer area (evaporator and preheater) than baseline R245fa, especially for Isobutane. However, its lower critical point narrows its application range, which is not extended to a higher heat source. R1233zd(E) and Isopentane present a close total heat transfer area, especially under high temperature heat sources. From Fig. 4 it can also be noticed that as the heat source increases, the heat transfer area variation of the preheater is more pronounced than that of the evaporator. This can be explained from Fig. 6. For the preheater, under different heat sources, the pinch point (5 K), water outlet temperature and working fluid inlet temperature does not change; thus, the logarithmic mean temperature difference (LMTD) does not vary. However, for the evaporator, as

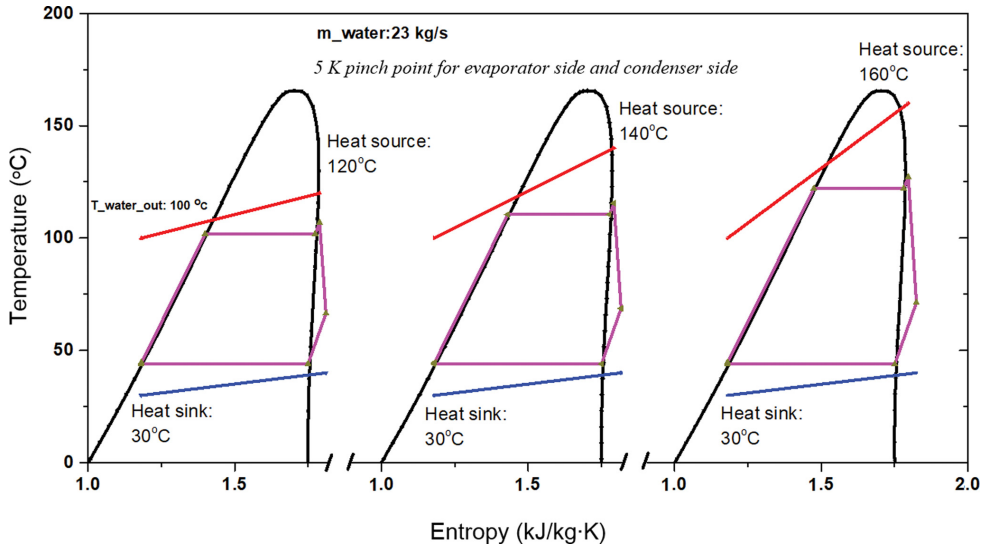

Fig. 6. T-s diagrams for different heat sources for R1233zd(E).

the heat source inlet temperature increases, it is easily predicted LMTD increases, leading a lower heat transfer area percentage for the two-phase domain.

Fig. 5 shows the condenser side (condenser and desuperheater) heat transfer area performance under different refrigerants. In general, R245fa exhibits a slightly lower total heat transfer area than other fluids. The two phase domain takes more than 85% of the capacity and the left is the gas phase. Due to the poor refrigerant gas state/water liquid state heat transfer characteristics of the desuperheater, its heat transfer area is even comparable to that of the two-phase condenser under the 120 °C heat source level. As the heat source increases, the two phase condenser heat transfer area increase is more pronounced than the desuperheater. Similarly, it can be explained from Fig. 6. The temperature profile for the condenser does not change with a raised heat source, while that for the desuperheater varies, with an increased refrigerant inlet temperature, leading a larger LMTD. Accordingly, the heat transfer area increase of the desuperheater is not that pronounced. In addition, a comparison between Fig. 4 and Fig. 5 indicates that the condenser side heat transfer area is much lower than evaporator side area.

2-2. Turbines

In this section, the turbine performance is discussed. In Fig. 7, the turbine volumetric flow ratio V_R and turbine size parameter SP under different refrigerants are displayed. Under the same heat source, R245fa displays the highest volume flow ratio, indicating a large change in rotor blade height between the inlet and outlet points should be made for the expansion process. Under the heat source of 120 °C, R1233zd(E) and Isopentane can produce a ~10% volume flow ratio reduction from baseline R245fa, n-Pentane gives a ~5% reduction, and Isobutane can even achieve a 17% decrease, respectively. Similar trend can be found for other heat sources. For the size parameter SP, i.e., the turbine size indicator, only Isobutane has a lower value than R245fa. Under the same heat source,

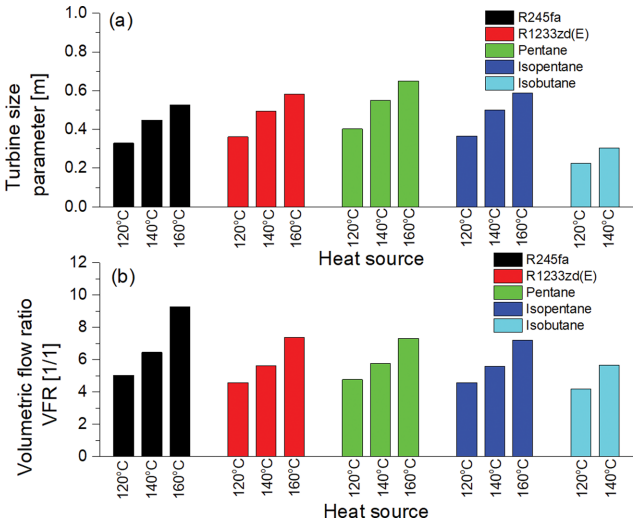

Fig. 7. Turbine performance under different refrigerants.

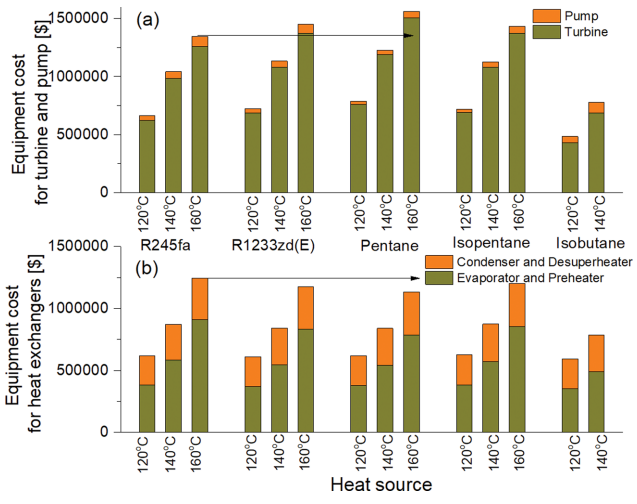

Fig. 8. Organic Rankine cycle component cost under different refrigerants.

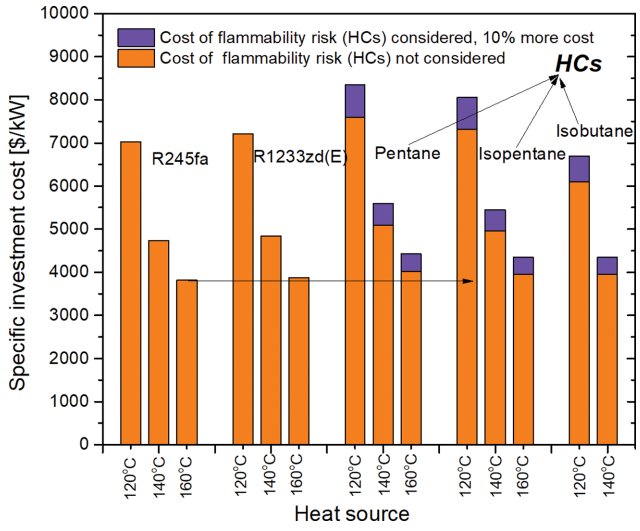

Fig. 9. Organic Rankine cycle specific investment cost under different refrigerants.

compared with R245fa, an SP increase of ~10% for R1233zd(E), ~22% for n-Pentane, and ~11% for Isopentane can be achieved, respectively. A decrease of 32% Isobutane can be obtained, indicating a higher cost saving for turbine size than other fluids.

3. ORC Component Cost and System Specific Investment Cost

This section discusses the ORC component cost and system SIC. Fig. 8 shows the component cost under different refrigerants. The condenser side heat exchanger cost is lower than the evaporator side. All R245fa alternatives exhibit a lower total heat exchanger cost from baseline R245fa. Take the heat source of 140 °C, for example: a heat exchanger cost drop of 3.6%, 4.0%, 0.8% and 9.8% can be attained for R1233zd(E), n-Pentane, Isopentane, and Isobutane, respectively. Regarding the turbine and pump cost, all alternatives hold a higher value than R245fa except Isobutane. Under the heat source of 140 °C, an increase of 8.5%, 17.5% and 7.8% can be obtained from the baseline for R1233zd(E), n-Pentane, and Isopentane, respectively. Isobutane shows ~25% turbine and pump cost reduction, due to its lower turbine size parameter SP.

The system SIC is shown in Fig. 9. It can be found that only Isobutane holds a lower value than R245fa. However, its lower critical temperature narrows its application and it cannot be extended its use for a higher heat source. Among the other three alternatives, (R1233zd(E), n-Pentane, Isopentane), R1233zd(E) displays the lowest value, for both two scenarios, with or without risk of flammability cost considered. Under the heat source temperature of 140 °C, R1233zd(E) only exhibits 2.3% higher SIC than the baseline R245fa. For the scenario of flammability risk cost not considered, n-Pentane and Isopentane display ~8% and ~4.5% SIC increase, respectively; with the flammability risk cost not considered, they can exhibit more than 15% SIC rise. Increasing the heat source gives significant SIC reduction, ~33% reduction from 120 °C to 140 °C, and ~46% drop from 120 °C to 160 °C, respectively. In fact, in the current version only 10% more cost is assumed for the A3 fluids for flammability risk, and in practical application, more cost concerning installation and maintenance aspects can add more burden for ORC plant built-up. Thus, from the thermo-economic scale with an extended application range, R1233zd(E) exhibits a better overall performance index when compared with other R245fa alternatives.

CONCLUSIONS

Evaluation of new low GWP fluids to replace R245fa for ORC plants is of high importance for practical applications. Most previous studies were only based on thermodynamic cycle analyses and did not give enough consideration for the component performance between the heat source/sink and corresponding fluids. The current study conducted the ORC thermo-economic evaluation of R1233zd(E) as R245fa alternative in comparison with other natural fluids n-Pentane, Isopentane, and Isobutane for geothermal application, from both the system level and component level aspects.

In this study, the heat source water flow rate remains constant and 5 K pinch point is pre-set for both evaporator side and condenser side. For the system level comparison, all working fluids have a close net thermal efficiency within 2%. Increasing the heat source from 120 °C to 160 °C gives more than 20% efficiency rise. Due to the lower critical temperature for Isobutane, 5 K pinch point does not exist at the evaporator side under the heat source of 160 °C. R1233zd(E) displays a close mass flow rate value (within 2%) to R245fa and other non-synthesized working fluids exhibit more than 40% flow rate reduction from the baseline.

For the component size aspects, all alternatives including R1233zd(E) can provide a lower total evaporator side heat transfer area (evaporator and preheater) than baseline R245fa, especially for Isobutane. The condenser side (condenser and desuperheater) heat transfer area is much lower than the evaporator side. R245fa exhibits slightly lower total condenser side heat transfer areas than other fluids. Different from the evaporator side, as the heat source increases, the two phase heat transfer area (i.e., condenser) increase is more pronounced than the single phase heat transfer area (i.e., desuperheater). R245fa displays the highest volume flow ratio, indicating a large change in rotor blade height between the inlet and outlet stations for the expansion process. For the size parameter SP, an increase of ~10% for R1233zd(E), ~22% for n-Pentane, and ~11% for Isopentane can be achieved, respectively. A decrease of 32% Isobutane can be obtained, indicating a higher cost saving for turbine size than other fluids. Such discoveries can quantitatively provide suggestions for the manufacturers to select the component size from their existing or new supplier database. For the component cost aspects, all R245fa alternatives exhibit a lower total heat exchanger cost. Regarding the turbine and pump cost, all alternatives hold a higher value than R245fa except Isobutane. Under a heat source of 140 °C, a rise of 8.5%, 17.5% and 7.8% can be obtained from the baseline for R1233zd(E), n-Pentane, and Isopentane, respectively. Isobutane shows ~25% turbine and pump cost reduction, due to its lower turbine size parameter SP.

Though Isobutane can achieve a close SIC to baseline R245fa, its lower critical temperature restricts its use for higher heat sources. Except Isobutane, R1233zd(E) only exhibits ~2.3% higher cost than the baseline R245fa while others exhibit more than 15% cost rise. Thus, from the thermo-economic scale with an extended application range, R1233zd(E) exhibits a better overall performance index when compared with other R245fa alternatives and can serve as a

promising candidate to replace R245fa.

NOMENCLATURE

Abbreviations

CEPEI : chemical engineering plant cost index
EORC : organic Rankine cycle with a vapor-liquid ejector
EU : european union
GHG : greenhouse gas
GWP : global warming potential
HC : hydrocarbon
HCFC : hydrochlorofluorocarbon
HFC : hydrofluorocarbon
HFO : hydrofluoroolefin
HP : heat pump
LMTD : logarithmic mean temperature difference
NBP : normal boiling point
ODP : ozone depletion potential
ORC : organic Rankine cycle
RORC : regenerative organic Rankine cycle
SIC : specific investment cost

Symbols

A : area [m^2]
C : cost [$] or coefficient for the component cost functions [-]
d : tube diameter [m]
D_s : shell diameter [m]
f : friction factor
$\dot{G}$: mass velocity [kg/m^2s]
h : enthalpy per unit mass of the state [kJ/kg] or heat transfer coefficient [$W/m^2 \cdot K$]
k : thermal conductivity [W/m·K]
K : coefficient related to the component or coefficient related to the shell-and-tube geometry
L : length [m]
LMTD : log-mean temperature difference [°C]
M : refrigerant charge amount [kg]
$\dot{m}$: refrigerant mass flow rate [kg/s]
P : pressure of the state [kPa or bar]
P_r : Prandtl number
P_T : tube pitch [mm]
$\dot{Q}$: heat delivery/flow [kW]
Re : Reynold number
SP : turbine size indicator [m^2]
SIC : specific investment cost [$/kW]
U : heat transfer coefficient [$W/m^2 \cdot K$]
V : volume flow rate [m^3/s]
W : power consumption/generation [kW]
ω : flammability factor, for non-flammable refrigerants, it is 1 and for flammable refrigerants, it is pre-set as 1.1
Y^2 : Chisholm parameter [-]
φ : the turbine size ratio [-]
α : void fraction[-]
x : quality [kg/kg]
ρ : density [kg/m^3]
η : net thermal efficiency
δ : relative area ratio [-]

Subscripts

p : pump
s : shell
t : turbine or tube
g : gas
HX : heat exchanger
in : inlet
l : liquid
v : vapor
out : outlet
ref : refrigerant
tp : two phase
1-4 : state point

REFERENCES

1. EU climate action, https://ec.europa.eu/clima/citizens/eu_en (2021).
2. M. Davis, A. Moronkeji, M. Ahiduzzaman and A. Kumar, *Energy Sustain. Dev.*, **59**, 243 (2020).
3. U. Muhammad, M. Imran, D. H. Lee and B. S. Park, *Energy Convers. Manag.*, **103**, 1089 (2015).
4. M. Li, J. Wang, W. He, L. Gao, B. Wang, S. Ma and Y. Dai, *Renew. Energy*, **57**, 216 (2013).
5. G. Li, *Sustain. Energy Technol. Assess.*, **21**, 33 (2017).
6. G. Li, *Korean J. Chem. Eng.*, **38**, 1438 (2021).
7. The European Parliament and the Council of the European Union, Regulation (EU) no 517/2014 of the European parliament and the council of the European union of 16 April 2014 on fluorinated greenhouse gases and repealing regulation (EC) No. 842/2006 (2014).
8. W. Liu, D. Meinel, C. Wieland and H. Spliethoff, *Energy*, **67**, 106 (2014).
9. F. Moles, J. Navarro-Esbrí, B. Peris, A. Mota-Babiloni, A. Barragan-Cervera and K. K. Kontomaris, *Appl. Therm. Eng.*, **71**, 204 (2014).
10. F. Moloney, E. Almatrafi and D. Y. Goswami, *Renew. Energy*, **147**, 2874 (2020).
11. J. Chen, Y. Huang, Z. Niu, Y. Chen and X. Luo, *Energy Convers. Manag.*, **157**, 382 (2018).
12. G. A. Longo, S. Mancin, G. Righetti, C. Zilio and J. S. Brown, *Appl. Therm. Eng.*, **167**, 114804 (2020).
13. A. Giuffrida, *Energy*, **161**, 1172 (2018).
14. A. Mahmoudi, M. Fazli and M. R. Morad, *Appl. Therm. Eng.*, **143**, 660 (2018).
15. B. V. Datla and J. J. Brasz, Comparing R1233zd and R245fa for low temperature ORC application, in: 15th International Compressor Engineering Cornference at Purdue, 14-17 July, 2014 (2014)
16. S. Eyerer, C. Wieland, A. Vandersickel and H. Spliethoff, *Energy*, **103**, 660 (2016).
17. F. Molés, J. Navarro-Esbrí, B. Peris and A. Mota-Babiloni, *Appl. Therm. Eng.*, **98**, 954 (2016).
18. J. Yang, Z. Sun, B. Yu and J. Chen, *Appl. Therm. Eng.*, **141**, 10 (2018).
19. J. Yang, Z. Ye, B. Yu, H. Ouyang and J. Chen, *Energy*, **173**, 721 (2019).
20. S. Eyerer, F. Dawo, J. Kaindl, C. Wieland and H. Spliethoff, *Appl.*

Energy, **240**, 946 (2019).
21. L. Talluri, O. Dumont, G. Manfrida, V. Lemort and D. Fiaschi, *Appl. Therm. Eng.*, **174**, 115293 (2020).
22. L. Talluri, O. Dumont, G. Manfrida, V. Lemort and D. Fiaschi, *Energy*, **211**, 118570 (2020).
23. E. Lemmon, M. Huber and M. Mclinden, NIST reference fluid thermodynamic and transport properties REFPROP, version 10.0. The National Institute of Standards and Technology (NIST) (2021).
24. Y. A. Çengel, *Heat and mass transfer* (Second ed.), McGraw-Hill (2002).
25. D. Q. Kern, Process heat transfer, Tata McGraw-Hill Education, New York (1950).
26. D. Green and R. Perry, *Perry's chemical engineers' handbook*, McGraw-Hill, New York (2007).
27. W. H. McAdams, *Heat transmission*, McGraw-Hill, New York (1958).
28. T. Tinker, *Proceedings of the general discussion on heat transfer*, Institution of Mechanical Engineers, London (1951).
29. G. F. Hewitt, *Hemisphere handbook of heat exchanger design*, Hemisphere Publishing Corporation, New York (1990).
30. L. D. Boyko and G. N. Kruzhilin, *Int. J. Heat Mass Tran.*, **10**, 361 (1967).
31. E. Macchi, *Design criteria for turbines operating with fluids having a low speed of sound in closed cycle gas turbines. Lecture series 100 on closed cycle gas turbines*, von Karman Institute for Fluid Dynamics (1977).
32. S. L. Dixon, *Fluid mechanics and thermodynamics of turbomachinery*, 4th Ed. Butterworth-Heinemann (1998).
33. D. Japikse and N. C. Baines, *Introduction to turbomachinery*, 1st Ed. Concepts ETI, Inc. and Oxford University Press (1997).
34. R. Turton, R. C. Bailie, W. B. Whiting and J. A. Shaeiwitz, *Analysis, synthesis and design of chemical processes*, Pearson Education (2008).
35. Chemical Engineering Plant Cost Index, http://www.chemengonline.com/pci-home, Chemecal Engineering (2020).